International Journal of Greenhouse Gas Control 46 (2016) 240–247

Contents lists available at ScienceDirect

International Journal of Greenhouse Gas Control

journal homepage: www.elsevier.com/locate/ijggc

Experimental investigation of the effect of carbon dioxide on *Pseudomonas putida* biofilms in a two-dimensional glass network micromodel

Varvara Sygouni[a], Ioannis D. Manariotis[a], Constantinos V. Chrysikopoulos[b,*]

[a] Department of Civil Engineering, University of Patras, 26500 Patras, Greece
[b] School of Environmental Engineering, Technical University of Crete, 73100 Chania, Greece

ARTICLE INFO

Article history:
Received 5 November 2015
Received in revised form 8 January 2016
Accepted 12 January 2016

Keywords:
Biofilm
Pseudomonas putida
CO_2
Micromodel
Pore network
Permeability

ABSTRACT

Capturing and storing carbon dioxide (CO_2) emissions in properly selected deep geologic formations is considered a promising solution for the reduction of CO_2 in the atmosphere. However, potential CO_2 leakage from a storage geologic formation is a major concern. In this work, the impact of CO_2 on biofilm formations is examined experimentally. In order to estimate the effect of CO_2 on biofilm formation, *Pseudomonas putida* biofilm was developed in a glass-etched pore network micromodel, where CO_2 injections were conducted. The transient growth of biofilm was monitored by taking high-resolution digital snapshots at various times. Biofilm and gas saturations of the micromodel were determined by binary image analysis of the various snapshots recorded. The observed biofilm breakdown due to CO_2 injection was discussed. It was shown that a CO_2 release affects only temporarily the *P. putida* biofilm. Also, biofilm age is significant to biofilm breakdown, because denser biofilm (fully developed) near the inlet of the pore network is affected less by a CO_2 release.

1. Introduction

Geological storage of carbon dioxide (CO_2) in deep geologic formations (e.g. depleted oil and gas reservoirs, deep aquifers) is considered as a promising solution for reduction of CO_2 emissions to the atmosphere, and elimination of the greenhouse effect (IPCC, 2005). Nevertheless, fluid pressure will increase in storage reservoirs in response to CO_2 injection under supercritical conditions. This increase, combined with buoyancy, may result in upward migration of CO_2 through leakage pathways (Mitchell et al., 2009; Humez et al., 2011). Leakage of CO_2 is a problem of great importance because elevated CO_2 concentrations are expected to reduce the aqueous solution pH, which may affect the minerology, chemical composition, and microbial activity of potable groundwater (Zhang et al., 2006; Zheng et al., 2009; Kharaka et al., 2009; Apps et al., 2010; Humez et al., 2013; Carroll et al., 2014).

Although bacteria films have been observed as early as 1939 by several researchers (ZoBell, 1939, 1943; Wattle, 1942; Butterfield and Wattle, 1941; Cooke, 1959; Wood, 1967; Corpe, 1970; Matson and Characklis, 1976), the term "biofilm" was initially introduced in the literature only in 1975 by Mack et al. (1975). Biofilm is a complex three-dimensional structure of bacteria communities. When bacteria are attached on a submerged surface, extracellular polymeric substances (EPS) are produced during the progressive colonization of the surface. Worthy to note is that biofilms grow practically everywhere, including: forests, deserts, deep oceans, soils, plants, and human body (Costerton et al., 1994). Several experimental and numerical studies published in the literature have proposed various possible mechanisms of biofilm growth (Stewart and Kim, 2004; Kapellos et al., 2007; Kim et al., 2010). The growth of biofilms within porous materials (e.g. soil, rocks, filters) results in permeability reduction, which is known as "bioclogging" (Thullner et al., 2002; Glatstein and Francisca, 2014).

Cell activity is strongly affected by dissolved CO_2 (Zhang et al., 2006), because high CO_2 concentrations may result in cell inactivation (Bertoloni et al., 2006), which is more pronounced with increasing pressure and temperature (Oule et al., 2006). Note that sudden changes in pH have a relatively small effect on biofilms (Kirk et al., 2012). However, experiments in bioreactors have shown that several Fe(III) and SO_4^{2-} reducing microorganisms are affected by CO_2 (Kirk et al., 2013).

In some cases, such as in wetland wastewater treatment (Langergraber et al., 2003; Nivala et al., 2012; Hua et al., 2014) or dental hygiene (Wang et al., 2014; Al-Ahmad et al., 2014), the

Abbreviations: BSD, biofilm saturation decrease; cfu, colonies forming units; ddH_2O, distilled deionized water; EPS, extracellular polymeric substances.

* Corresponding author.
E-mail address: cvc@enveng.tuc.gr (C.V. Chrysikopoulos).

http://dx.doi.org/10.1016/j.ijggc.2016.01.016
1750-5836/

Nomenclature

A_m	cross-sectional area to flow (L^2)
D_p	pore depth (L)
k	intrinsic permeability (L^2)
L_m	pore network length (L)
L_p	pore length (L)
Q	total flow rate ($L^3\,t^{-1}$)
$\mathbf{V}_{co_2}$	volume of CO_2 leaked in units of [mL] (L^3)
W_m	pore network width (L)
W_p	pore width (L)
ΔP	total pressure drop (Pa) ($Mt^{-2}\,L^{-1}$)
Δx	separation distance between pressure transducers (L)
μ	fluid viscosity (Pa s) ($Mt^{-1}\,L^{-1}$)

existence of bacteria and biofilms are undesirable, there are several engineering applications where biofilms are most useful. Biofilms are often employed in enhanced oil recovery (Soudmand-asli et al., 2007; Sen, 2008), in landfills as barriers, in biofilters, soil remediation and bioremediation (Seki et al., 1998; James et al., 2000), and for CO_2 leakage reduction (Mitchell et al., 2009, 2010; Ebigbo et al., 2010; Cunningham et al., 2011; Manceau et al., 2014; Phillips et al., 2012; Sygouni et al., 2015).

The aim of this study was to use well-established non-invasive visualization procedures (e.g. Jia et al., 1999; Corapcioglu and Fedirchuk, 1999; Tsakiroglou et al., 2003; Chrysikopoulos and Vogler, 2006; Werth et al., 2010; Thomas and Chrysikopoulos, 2010) to investigate the effect of gas CO_2 on *Pseudomonas putida* biofilms. Visualization experiments of CO_2 injections in a glass-etched micromodel containing *P. putida* biofilm were performed. The effect of CO_2 on *P. putida* biofilms was investigated by taking and analyzing a series of high-resolution snapshots of the pore network micromodel. During the flow-through experiments, pH and bacteria concentration of the effluent were measured. Also, biofilm growth and biofilm corruption after the CO_2 injection were monitored. To the best of our knowledge, no previous study has investigated the effect of gas CO_2 on *P. putida* biofilm within a glass-etched pore network micromodel.

2. Methods and materials

2.1. Pore network and glass micromodel

The glass micromodel used in this study was constructed using the photolithographic technique developed by McKellar and Wardlaw (1982) with certain modifications initially proposed by Payatakes and co-workers (Vizika and Payatakes, 1989; Avraam et al., 1994; Avraam and Payatakes, 1995) and subsequently implemented by numerous investigators (Tsakiroglou et al., 2003; Chrysikopoulos et al., 2011; Robin et al., 2012). Briefly, a pore network with length, L_m = 18 cm, and width, W_m = 11 cm, was carefully designed and printed on a transparent sheet of acrylic film, to create the photographic "mask" (see Fig. 1a). Two pieces of mirror glass were placed in a 7.97 M NaOH solution bath for a 12 h, to expose the copper. The mirrors were placed in a dark room and the copper surfaces were sprayed with positive photoresist (Cramolin, Germany). After the positive photoresist was dried in an oven at 50 °C for 15 min, the negative film of the network "mask" was carefully placed on top of the positive photoresist film, and the glass essays were exposed to UV for 45 min, so that the visible positive photoresist film was polymerized. The glass essays were placed in a 0.16 M NaOH solution bath for approximately 1 min to dissolve the non-polymerized positive photoresist film. Subsequently, the

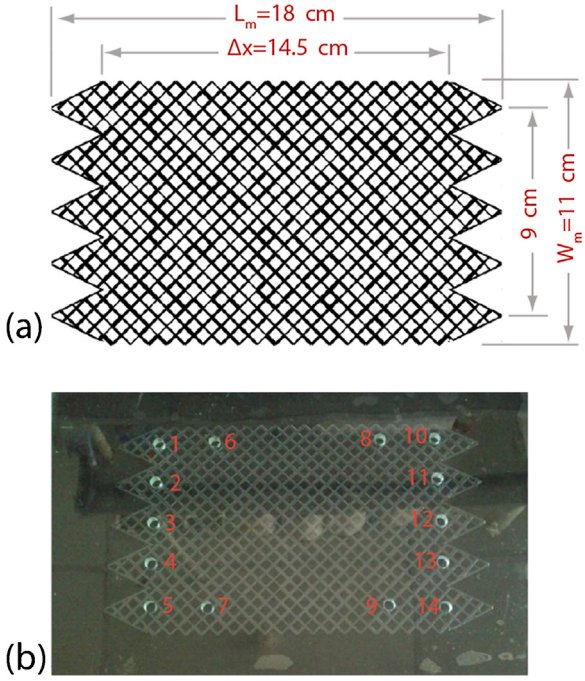

Fig. 1. (a) Image (mask) of the pore network micromodel, where the dark areas correspond to micromodel voids. (b) The glass pore-network micromodel used in this study.

glass essays were washed with H_2O and placed in a HNO_3 solution bath (200 mL HNO_3 65% and 200 mL distilled deionized water (ddH_2O)) for just a few seconds to dissolve the copper surface area unprotected by the positive photoresist film. Then, the glass essay of the pore network, which should not be etched, was waxed with warm paraffin. Subsequently, an HF solution (75 mL HF 90% in 25 mL ddH_2O) was poured onto the waxed glass essay for 5 min. The glass essays were washed with H_2O and the wax was removed mechanically. Then the glass essays were placed in a HNO_3 solution (200 mL HNO_3 in 230 mL ddH_2O) until all of the remaining copper was removed. Next, the various inlet and outlet ports were drilled. Finally, the two etched glasses were sintered in a programmable furnace to produce the desired glass micromodel used in this study (see Fig. 1b).

The micromodel fabrication procedure employed in this work does not necessarily yield a pore network with spatially uniform pore depth D_p [L^2], pore width W_p [L^2], and pore length L_p [L^2]. It should be noted that this is not an important shortcoming for the present study, because the mean values of the pore depth, width, and length, $\bar{\mathbf{D}}_p = 172\,\mu m$, $\bar{\mathbf{W}}_p = 1220\,\mu m$, $\bar{\mathbf{L}}_p = 5560\,\mu m$, respectively, determined with procedures outlined by Tsakiroglou et al. (2003), can effectively be used. All structural properties of the micromodel used in this study are listed in Table 1.

Table 1
Micromodel structural properties.

Property	Symbol	Value (units)
Micromodel length	L_m	18.0 (cm)
Micromodel width	W_m	11.0 (cm)
Separation distance between inlet and outlet ports	Δx	14.5 (cm)
Mean pore width	$\bar{\mathbf{W}}_p$	1220 (μm)
Mean pore depth	$\bar{\mathbf{D}}_p$	172 (μm)
Mean pore length	$\bar{\mathbf{L}}_p$	5560 (μm)
Intrinsic permeability	k	281.9 (Da)[a]

[a] Da = darcy = 10^{-12} m^2.

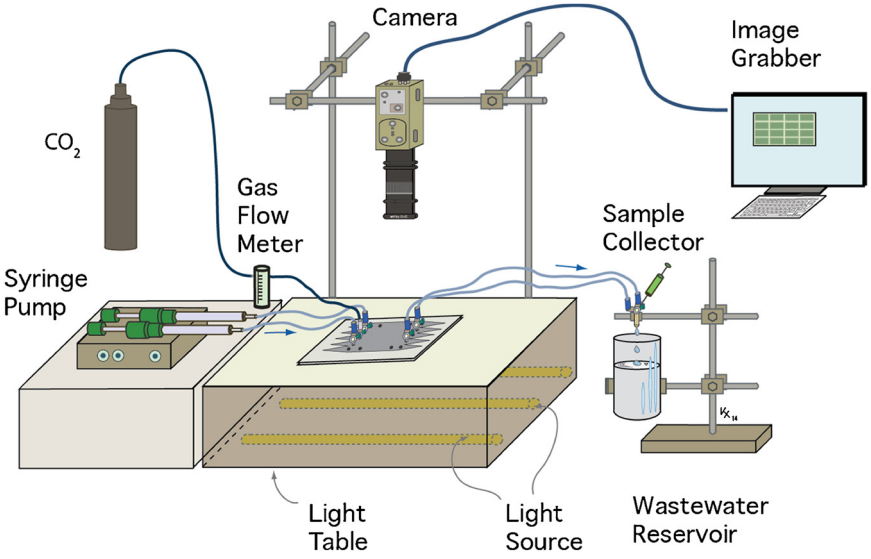

Fig. 2. Schematic illustration of the experimental setup.

2.2. Experimental apparatus

The main experimental setup consisted of the following principal apparatus: (i) the micromodel, (ii) a syringe pump (Cole-Parmer 74900), (ii) a custom-made light table equipped with three visible light lamps (Philips TLD graphica Pro 18 W/95), (iv) a color video camera with picture enhance controls (Sony HD 3-CCD, DXC-390P) mounted on a custom-made flexible stand, and (v) a personal computer equipped with a digital video recording (image grabber) software (NORPIX). The arrangement of the experimental apparatus is illustrated schematically in Fig. 2.

The micromodel was placed on top of light table and fluids were injected into the micromodel with the syringe pump. It should be noted that, although there were 14 ports available in the constructed micromodel (see Fig. 1b), only ports 2 and 4 were used for fluid inlets, whereas port 3 was used for CO_2 injection. The ports 11 and 13 were used as fluid outlets, whereas port 12 was used as a fluid outlet only during CO_2 injection. The outflow from ports 11 and 13, and occasionally port 12 (during CO_2 injection) were merged into a pH flow-through cell (EW-05662-48, Cole-Parmer) for determination of the pH of the effluent with a pH-meter (Inolab, WTW). Three way valves were installed before the inlet ports and after the outlet ports in order to isolate the porous medium when the syringes were refilled. Syringe filters of 0.45 μm pore size (Fitropur S 0.45, Sarstedt) were installed just before the inlet ports in order to barrier the bacteria from the nutrient in the syringe pump, because *P. putida* bacteria are motile with a tendency to move toward the nutrient. All other ports (namely ports 1, 5–10, 14 shown in Fig. 1b) were tightly sealed with silicon caps. Also, a precision regulator (RP1000-8-02-G49P, Bibus) was placed on the CO_2 gas cylinder line in order to control precisely the gas flow into the micromodel.

Before each experiment the glass network micromodel was cleaned using chromo-sulphuric acid and subsequently, washed out several times with ddH_2O. Ethyl alcohol was injected into the micromodel and it was placed overnight in an oven at 37 °C. Finally, to remove ethyl alcohol, the micromodel was flushed several times with nutrient at a flow rate of $Q \sim 2$ mL/min. After the bacteria injection, formation and growth of the biofilm was monitored by taking snapshots and videos of the glass network micromodel at various resolutions. Fluid samples were collected at the outlet of the porous medium periodically to determine the concentration of the bacteria. Furthermore, biofilm and fluid saturation levels within the glass network micromodel were determined by performing image analysis of the recorded snapshots. MATLAB® was used to binarize the images, re-color the void areas occupied with gas, and compare them to the void areas occupied with biofilm.

2.3. Micromodel intrinsic permeability

For the estimation of the intrinsic permeability of the glass micromodel, a low differential pressure transducer (Omega PX154) equipped with a data acquisition system (OM-USB-1208FS and TracerDAQ Pro software) was connected to ports 3 and 12 (see Fig. 1a), in order to measure the pressure drop across the medium for varying flow rates. Based on Darcy's law, the intrinsic permeability is defined as (Bear, 1972):

$$k = -\mu \frac{\Delta x}{A_m} \left(\frac{Q}{\Delta P} \right) \quad (1)$$

where Q [$L^3\,t^{-1}$] is the total flow rate k [L^2] is the intrinsic permeability, $A_m = W_m \times \overline{D}_p$ [L^2] is the cross-sectional area to flow, ΔP [$M/(t^2\,L)$] is the total pressure drop over a micromodel length Δx [L], which is equal to the separation distance between the two pressure transducers installed on the plastic tubes inserted into ports 3 and 12 using three way valves ($\Delta x = 14.5$ cm), and μ [M/(t L)] is the viscosity of the fluid. The value of the term $\Delta P/Q$ is determined by constructing a plot of observed pressure drop versus flow rate, and calculating the slope of the experimental data.

2.4. Bacteria and biofilm

P. putida was used for the development of biofilm, which was cultured and collected at the laboratory following the procedures outlined by Vasiliadou and Chrysikopoulos (2011). Briefly, *P. putida* was cultured in 10 mL of nutrient broth (Laury Pepto Bios Broth 35.6 g/L, Biolife Italiana Srl, with typical composition of tryptone ($C_4H_{11}NO_3{\cdot}HCl$): 20 g/L, lactose ($C_{12}H_{22}O_{11}$): 5 g/L, sodium chloride (NaCl): 5 g/L, sodium-lauryl-sulfate ($C_{12}H_{26}{\cdot}NaSO_4$): 0.1 g/L, dipotassium-hydrogen-phosphate (K_2HPO_4): 2.75 g/L, and potassium-dihydrogen-phosphate (KH_2PO_4): 2.75 g/L) for 20 h at 30 °C in an orbital shaker (Innova 43, New Brunswick Scientific, NJ) at 140 rpm. A culture volume of 5 mL was transferred in 250 mL of the nutrient broth and it was re-cultured for 20 h at 30 °C and 140 rpm. Finally, bacteria were collected by centrifugation for 8 min at 10,000 rpm (SL40R, Thermo Scientific), washed out several times

with ddH_2O and subsequently, washed out once more with sterile saline before they were stored in sterile saline at 4 °C. Prior to injection of the culture into the pore network, *P. putida* cells were diluted in nutrient broth to the desired concentration of approximately 10^7 to 10^8 cfu/mL. The pH of the injection culture was pH = 7.1.

The concentration of *P. putida* in the effluent of the glass network micromodel was measured using the spread plate technique by inoculating 0.1 mL of aliquots in Petri dishes containing sterile Agar (Lab-Agar™ PS 133, with typical composition of pancreatic digest of gelatin: 20.0 g//L, magnesium chloride ($MgCl_2$): 1.4 g/L, potassium sulfate (K_2SO_4): 1.0 g/L, cetrimide ($C_{17}H_{38}BrN$): 0.3 g/L, and agar: 13.6 g/L). Colonies were measured after incubation of Petri dishes in an incubator chamber (GCA Corporation/Precision Scientific Group, IL) at 37 °C for 48 h (see Fig. 3).

Two sets of experiments were conducted at room temperature (~25 °C). For the first experiment, bacteria with initial concentration of 4×10^8 cfu/mL were injected in the thoroughly cleaned micromodel. Approximately, 3 h later, the injection of nutrient broth at a constant flow rate of $Q = 0.00366$ mL/min was initiated. It should be noted that the 3-h delay period was necessary in order for the bacteria to attach onto the glass surface.

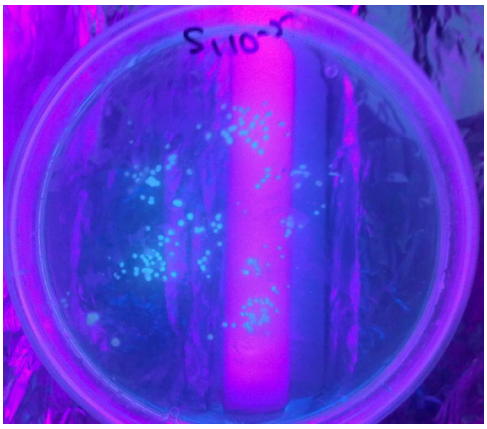

Fig. 3. A Petri dish with *P. putida* colonies over fluorescent lighting.

3. Experimental results and discussion

Fig. 4a presents three pore level snapshots at various times, whereas Fig. 4b presents three network level snapshots at various times. The observed bubbles are CO_2 gas produced due to organic matter consumption by *P. putida* cells. Note that after approximately four days of nutrient injection in the pore network micromodel, biofilm growth is becoming clearly visible (see Fig. 4a and b).

Biofilm development was first noticed near the inlet ports 2 and 4, where the nutrients are introduced into the micromodel. This is the reason that denser and thicker biofilm was developed near the inlet rather than the outlet of the pore network. Thicker

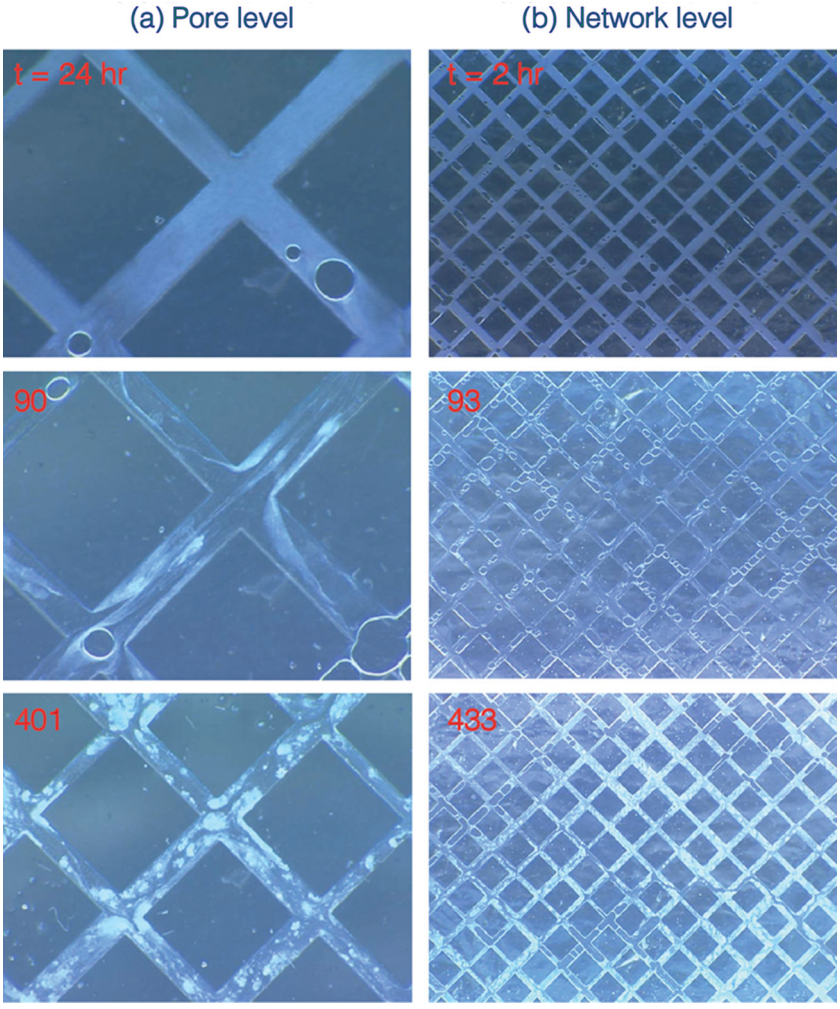

Fig. 4. Snapshots of biofilm formation and biochemically produced CO_2 taken before the injection of CO_2 at various times at the: (a) pore level and (b) network level.

Table 2
Volume of CO_2 used for each injection step.

Injection step	Time (h)	Injected CO_2 (mL)
1	431.3	15.0
2	574.9	3.0
3	600.4	0.045
4	667.7	0.1
5	691.8	0.068
6	739.8	0.03

and denser biofilm was developed near the micromodel inlet area, because this area was accessed first by the nutrients. When no significant changes were observed on biofilm's structure (after 430 h of experimental time), six successive relatively short time-period injections of gaseous CO_2 were performed using constant flow rate. Also, the chosen CO_2 injection time-periods were arbitrary, but progressively smaller, because the biofilm volume within the micromodel was progressively reduced. The preselected times of injection, together with the corresponding volumes of CO_2 injected are listed in Table 2.

Snapshots of the pore network, "before" and "after" each CO_2 injection, were recorded and presented in Fig. 5. Careful comparison of "before" and "after" snapshots reveals that there is some biofilm breakdown, and significant formation of CO_2 gas bubbles during each of the six injection steps. The effluent *P. putida* concentration was measured during each CO_2 injection period, whereas the effluent pH values were measured before and after each CO_2 injection. The experimental data are graphically illustrated in Fig. 6. As shown in Fig. 6, shortly after each CO_2 injection the pH of the effluent was decreased. This is an expected result, because when CO_2 is dissolved in the nutrient broth within the pores of the micromodel, it reacts with water to form carbonic acid (H_2CO_3), which rapidly looses protons and dissociates to bicarbonate (HCO_3^-) and hydrogen ions (H^+), and in turn HCO_3^- dissociates to carbonate (CO_3^{2-}) and H^+ (Stumm and Morgan, 1981):

$$CO_{2(g)} \Leftrightarrow CO_{2(aq)} \quad (2)$$

$$CO_{2(aq)} \Leftrightarrow H_2O \Leftrightarrow H_2CO_3 \quad (3)$$

$$H_2CO_3 \Leftrightarrow HCO_3^- + H^+ \quad (4)$$

$$HCO_3^- \Leftrightarrow CO_3^{2-} + H^+ \quad (5)$$

Significant carbonate activity (Eq. (5)) is unlikely to occur at the present experimental conditions (room temperature and pH < 8.3). The liberated protons or increase in H^+ concentration caused by each CO_2 short time-period injection leads to the observed $pH = -\log_{10}[H^+]$ decrease. Note that this pH reduction is only temporary because after each CO_2 injection the previously reduced pH increases again as soon as the supply of nutrients continues, and the CO_2 saturation of the pore network decreases.

The CO_2 concentration in the pore network decreases due to partial pressure reduction caused from fluid displacement by the nutrient flow, and by buffering reactions that also consumed CO_2. Fig. 6 indicates that the effluent *P. putida* concentration decreased by approximately five orders of magnitude shortly after the second CO_2 injection into the micromodel. This is mainly attributed to biofilm detachment, and possible stress of the bacterial cells by the injected CO_2. Note that CO_2 partial pressure increases have been reported in the literature to reduce bacterial growth (Motegi et al., 2013). The detached biofilm was subsequently displaced out from the micromodel by the interstitial flow. Note that the first two volumes of CO_2 injected into the micromodel were largest (see Table 2). Therefore, there was not enough time for the biofilm to sufficiently regrow within the pore network prior to the third injection step. Consequently, the effluent *P. putida* concentration after the third injection step was drastically reduced. However,

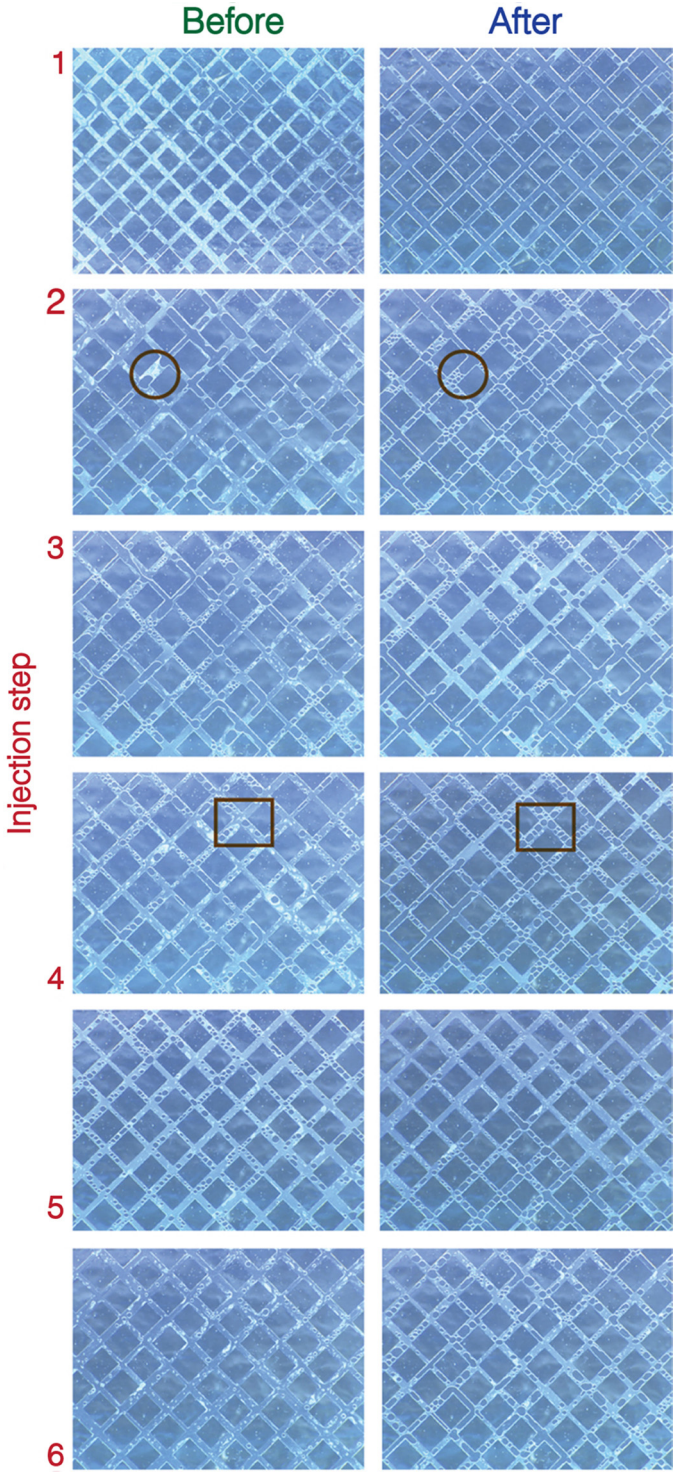

Fig. 5. Snapshots of the pore network taken before and after each of the six CO_2 injection steps. The inserted circles highlight the biofilm breakdown during injection step 2, and the squares the significant formation of gas bubbles during injection step 4.

after the abrupt reduction in biofilm mass, the biofilm progressively regrew and in turn the effluent *P. putida* concentrations progressively increased (see Fig. 6).

Analyzing the numerous high-resolution, digital snapshots of the micromodel, collected at various times during the experiment (including the snapshots shown in Fig. 5), the corresponding biofilm and gas saturations of the pore network were determined and presented graphically in Fig. 7. Clearly, it is evident from Fig. 7 that

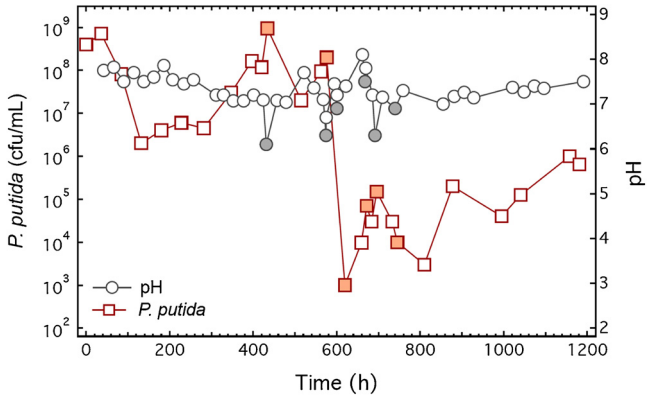

Fig. 6. Effluent *P. putida* concentration and pH versus time. The solid squares represent the effluent *P. putida* concentration during each CO_2 injection period and the solid circles represent the effluent pH shortly after each CO_2 injection.

shortly after each CO_2 injection, gas saturation of the pore network increased, whereas biofilm saturation of the pore network decreased. The observed decrease in biofilm saturation of the pore network shortly after each CO_2 injection was attributed to biofilm detachment and removal out from the micromodel. However, as shown in Fig. 7a, after the end of each CO_2 injection, the biofilm was regrown. Also, after completion of the injection steps, the biofilm was progressively regrown, and the biofilm saturation of the pore network steadily increased to its initial level. Figs. 6 and 7 show that, due to the strong buffering capacity of the nutrient, only a small pH decrease occurs during the CO_2 injection. Also, during the CO_2 injection, most of the nutrient occupying the small pore volume of the micromodel (~2.5 mL) was displaced. Consequently,

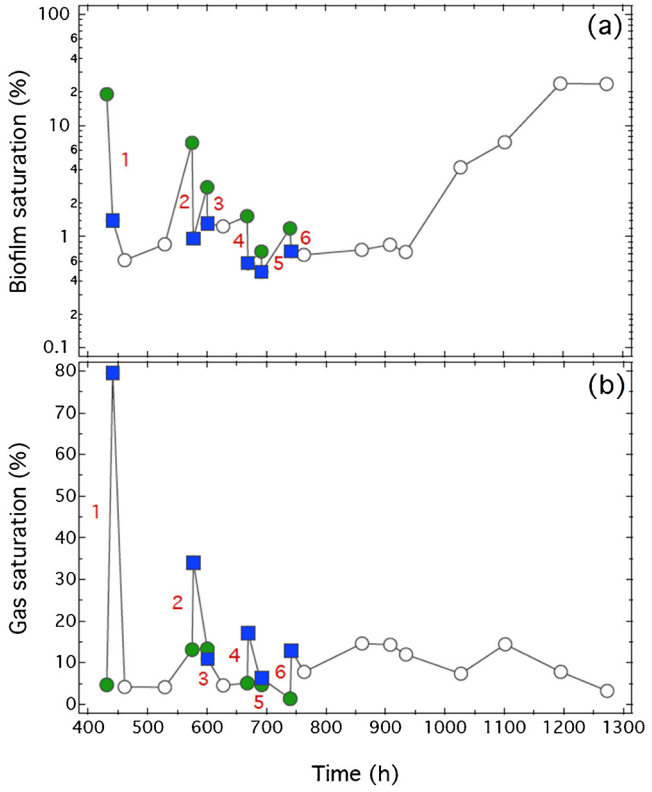

Fig. 7. Pore network saturation with: (a) biofilm and (b) gas versus time. The solid circles and solid squares represent the biofilm saturation of the pore network before and after the CO_2 injection, respectively. The numbers indicate the CO_2 injection step.

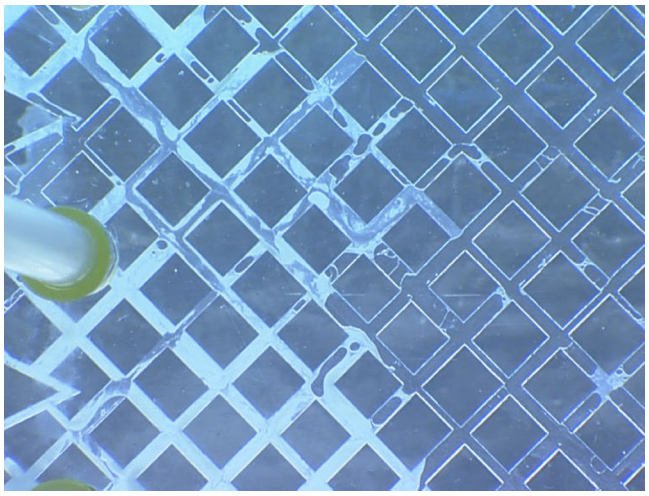

Fig. 8. A snapshot of the pore network near the inlet port 2, a few hours after the first CO_2 injection. Denser biofilm near the inlet port is not significantly affected by CO_2 injection.

the injected CO_2 gas displaced biofilm by the influence of shear forces, and that the small pH changes of the residual nutrient did not contribute to the observed biofilm destruction.

The observed increase in gas saturation of the pore network shortly after each CO_2 injection is intuitive, and strictly proportional to the volume of CO_2 injected. Note that the largest volume of CO_2 was injected during the first injection step (see Table 2), which is in perfect agreement with the results presented in Fig. 7b. It is worthy to note that the inlet ports of the network, where the biofilm is denser with stronger structure, CO_2 injection was relatively less destructive (see Fig. 8). This observation suggests that biofilm age can play a significant role to biofilm breakdown during CO_2 leakage. In Fig. 9 the observed biofilm saturation decrease is plotted against the volume of CO_2 injected (or leaked), and the following empirical correlation can be proposed:

$$BSD = 0.66 + 1.94V_{CO_2} - 0.054(V_{CO_2})^2 \quad (7)$$

where BSD [%] is the biofilm saturation decrease, and $\mathbf{V}_{CO_2}$ is the volume of CO_2 leaked in units of [mL]. Clearly, as expected, the smaller the volume of CO_2 released the smaller the biofilm destruction.

For the second experiment the initial concentration of the bacteria injected into the pore network was equal to 6×10^7 cfu/ml. The biofilm was slowly grown within the pores of the micromodel. At the 44th day of the experiment, no obvious changes on the biofilm's structure were noticable, the intrinsic permeability

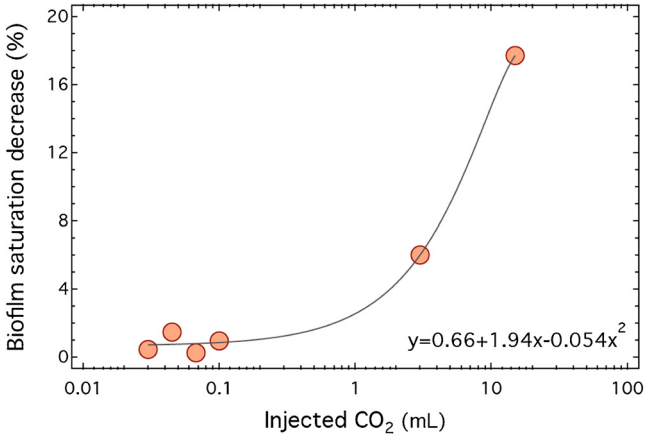

Fig. 9. Decrease of pore network biofilm saturation versus volume of CO_2 injected.

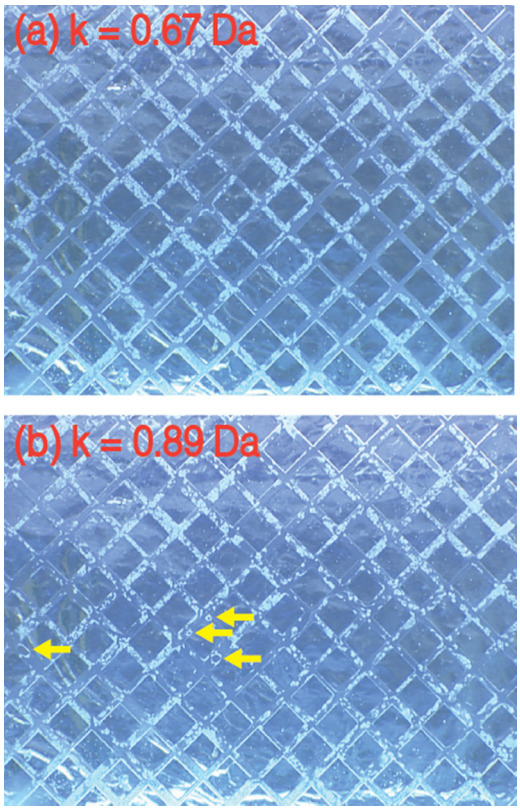

Fig. 10. Snapshots of the pore network: (a) before the CO_2 injection (here $k = 0.67$ Da), and (b) one day after the end of the CO_2 injection (here $k = 0.89$ Da). Note that only a few CO_2 gas bubbles are visible just one day past the CO_2 injection.

of the micromodel was determined to be $k = 0.67$ Da (where Da = darcy = 10^{-12} m^2) (see Fig. 10a), which corresponds to 99.8% reduction in the intrinsic permeability of the clean pore network micromodel ($k = 281.9$ Da). Then, CO_2 was injected into port 3 of the micromodel for approximately 1 h, at a flow rate of $Q = 0.15$ L/min, which contributed to abrupt detachment and displacement of a relatively large quantity of the biofilm. Worthy to note is that a portion of the injected CO_2 "short-circuited" the micromodel, creating distinct fingering between injection port 3 and the extraction port 12. Note that the injected CO_2 fingers break down to small bubbles due to local instabilities. This phenomenon is called "snap-off" and takes place when a wetting fluid displaces a non-wetting, depending on the ratio of the diameters of pore to throat and the fluid system wettability (Li and Wardlaw, 1986). It should be noted that there is always a thin film of nutrients and bacteria between the CO_2 gas and the glass surface, because the pore surfaces are not wetted by CO_2 gas (water-wet surfaces). The intrinsic permeability one day after the completion of the CO_2 injection, when no gas remained trapped in the micromodel, was also determined and it was found to be $k = 0.89$ Da (see Fig. 10b). Therefore, the CO_2 injection increased the diminished, due to biofilm growth (bioclogging), intrinsic permeability of the pore network micromodel by 32.8%. Only a few CO_2 gas bubbles are visible in Fig. 10b, suggesting that most of the CO_2 that remained within the micromodel during the injection period was displaced out from the micromodel by the interstitial flow and dissolved in the aqueous phase within just one day.

4. Conclusions

The experiments conducted in the glass-etched pore-network micromodel suggested that small quantities of CO_2 have relatively small effect on the *P. putida* biofilm. It was shown that CO_2 injections temporarily reduce the solution pH. Also, it was shown that CO_2 injections disrupt and partially breakdown the *P. putida* biofilm. However, this is only a temporary effect, because the biofilm was not destroyed completely and biofilm regrowth in the pore-network micromodel started immediately after each CO_2 injection step. Also, it was shown that biofilm age plays a significant role, because denser (fully developed) biofilm near the inlet of the micromodel was more resistant to breakdown during CO_2 injection. Finally, it was shown that a sudden CO_2 injection considerably enhanced the intrinsic permeability of the micromodel with *P. putida* biofilm, which soon returned to the level prior to the CO_2 injection. Therefore, a potential CO_2 leakage from a storage geologic formation is expected to impact only temporarily *P. putida* biofilm structures within potable water aquifers. The results of this study cannot be generalized for every biofilm type, because other biofilms (e.g. *Nitrosomonas*) are known to be influenced by pH reduction. Certainly, this work has improved our understanding of the impact of sudden and temporary CO_2 release on *P. putida* biofilm, but the question of what would be the long-term effects of continuous CO_2 release on biofilm growth remains unanswered.

Acknowledgments

This research has been co-financed by the European Union (European Social Fund-ESF) and Greek National Funds through the Operational program "Education and Lifelong Learning" under the action Thales (Project Geomecs). The authors are thankful to C.D. Tsakiroglou for generously providing the micromodel, to A.F. Aravantinou for laboratory assistance, and to M. Kornaros for providing the initial *P. putida* culture.

References

Al-Ahmad, A., Ameen, H., Pelz, K., Karygianni, L., Wittmer, A., Anderson, A.C., Spitzmuller, B., Hellwig, E., 2014. Antibiotic resistance and capacity for biofilm formation of different bacteria isolated from endodontic infections associated with root-filled teeth. J. Endod. 40 (2), 223–230.
Avraam, D.G., Payatakes, A.C., 1995. Flow regimes and relative permeabilities during steady-state two-phase flow in porous media. J. Fluid Mech. 293, 207–236.
Avraam, D.G., Kolonis, G.B., Roumeliotis, T.C., Constantinides, G.N., Payatakes, A.C., 1994. Steady-state two-phase flow through planar and nonplanar model porous media. Transp. Porous Med. 16, 75–101.
Apps, J.A., Zheng, L., Zhang, Y., Xu, T., 2010. Evaluation of potential changes in groundwater quality in response to CO_2 leakage from deep geologic storage. Transp. Porous Med. 82 (1), 215–246.
Bear, J., 1972. Dynamics of Fluids in Porous Media. Dover.
Bertoloni, G., Bertucco, A., De Cian, V., Parton, T., 2006. A study on the inactivation of micro-organisms and enzymes by high pressure CO_2. Biotechnol. Bioeng. 95 (1), 156–160.
Butterfield, C.T., Wattle, E., 1941. Studies of sewage purification: XV. Effective bacteria in purification by trickling filter. Pub. Health Rep. 56, 2445–2464.
Carroll, A.G., Przeslawski, R., Radke, L.C., Black, J.R., Picard, K., Moreau, J.W., Haese, R.R., Nichol, S., 2014. Environmental considerations for subseabed geological storage of CO_2: a review. Cont. Shelf Res. 83, 116–128.
Chrysikopoulos, C.V., Plega, C.C., Katzourakis, V.E., 2011. Non-invasive *in situ* concentration determination of fluorescent or color tracers and pollutants in a glass pore network model. J. Hazard. Mater. 189, 299–306.
Chrysikopoulos, C.V., Vogler, E.T., 2006. Acoustically enhanced ganglia dissolution and mobilization in a monolayer of glass beads. Transp. Porous Med. 64, 103–121.
Cooke, W.B., 1959. Trickling filter ecology. Ecology 40, 273–291.
Corapcioglu, M.Y., Fedirchuk, P., 1999. Glass bead micromodel study of solute transport. J. Contam. Hydrol. 36, 209–230.
Corpe, W.A., 1970. An acid polysaccharide produced by a primary film-forming marine bacterium. Dev. Ind. Microbiol. Am. Inst. Biol. Sci. 11, 402–412.
Costerton, J.W., Lewandowski, Z., DeBeer, D., Caldwell, D., Korber, D., James, G., 1994. Biofilms, the customized microniche. J. Bacteriol. 176, 2137–2142.
Cunningham, A.B., Gerlach, R., Spangler, L., Mitchell, A.C., Parks, S., Phillips, A., 2011. Reducing the risk of well bore leakage of CO_2 using engineered biomineralization barriers. Energy Proc. 4, 5178–5185.
Ebigbo, A., Helmig, R., Cunningham, A.B., Class, H., Gerlach, R., 2010. Modelling biofilm growth in the presence of carbon dioxide and water flow in the subsurface. Adv. Water Resour. 33, 762–781.
Glatstein, D.A., Francisca, F.M., 2014. Hydraulic conductivity of compacted soils controlled by microbial activity. Environ. Technol. 35 (15), 1886–1892.

Hua, G., Zeng, Y., Zhao, Z., Cheng, K., Chen, G., 2014. Applying a resting operation to alleviate bioclogging in vertical flow constructed wetlands: an experimental lab evaluation. J. Environ. Manag. 136, 47–53.
Humez, P., Audigane, P., Lions, J., Chiaberge, C., Bellenfant, G., 2011. Modeling of CO_2 leakage up through an abandoned well from deep saline aquifer to shallow fresh groundwaters. Transp. Porous Med. 90, 153–181.
Humez, P., Lagneau, V., Lions, J., Negrel, P., 2013. Assessing the potential consequences of CO_2 leakage to freshwater resources: a batch-reaction experiment towards an isotopic tracing tool. Appl. Geochem. 30, 178–190.
IPCC (Intergovernmental Panel on Climate Change), 2005. In: Metz, B., Davidson, O., de Coninck, H., Loos, M., Mayer, L. (Eds.), Special Report on Carbon Dioxide Capture and Storage. Cambridge University Press, Cambridge, UK/New York, NY, USA.
James, G.A., Warwood, B.K., Hiebert, R., Cunningham, A.B., 2000. Microbial barriers to the spread of pollution. In: Valdes, J.J. (Ed.), Bioremediation. Kluwer Academic, Amsterdam, The Netherlands, pp. 1–14.
Jia, C., Shing, K., Yortsos, Y.C., 1999. Visualization and simulation of non-aqueous phase liquids solubilization in pore networks. J. Contam. Hydrol. 35, 363–387.
Kapellos, G.E., Alexiou, T.S., Payatakes, A.C., 2007. A multiscale theoretical model for diffusive mass transfer in cellular biological media. Math. Biosci. 210, 177–237.
Kim, J.-W., Choi, H., Pachepsky, Y.A., 2010. Biofilm morphology as related to the porous media clogging. Water Res. 44, 1193–1201.
Kirk, M.F., Santillan, E.F.U., McGrath, L.K., Altman, S.J., 2012. Variation in hydraulic conductivity with decreasing pH in a biologically-clogged porous medium. Int. J. Greenh. Gas Control 11, 133–140.
Kirk, M.F., Santillan, E.F.U., Sanford, R.A., Altman, S.J., 2013. CO_2-induced shift in microbial activity affects carbon trapping and water quality in anoxic bioreactors. Geochim. Cosmochim. Acta 122, 198–208.
Kharaka, Y.K., Thordsen, J.J., Hovorka, S.D., Nance, S.H., Cole, D.R., 2009. Potential environmental issues of CO_2 storage in deep saline aquifers: geochemical results from the Frio-I brine pilot test, Texas, USA. Appl. Geochem. 24, 1106–1112.
Langergraber, G., Haberl, R., Laber, J., Pressl, G., 2003. Evaluation of substrate clogging processes in vertical flow constructed wetlands. Water Sci. Technol. 48 (5), 25–34.
Li, Y., Wardlaw, N.C., 1986. The influence of wettability and critical pore throat size ratio on snap-off. J. Colloid Interface Sci. 109, 461–472.
Mack, W.N., Mack, J.P., Ackerson, A.O., 1975. Microbial film development in a trickling filter. Microb. Ecol. 2, 215–226.
Manceau, J.-C., Hatzignatiou, D.G., de Lary, L., Jensen, N.B., Réveillère, A., 2014. Mitigation and remediation technologies and practices in case of undesired migration of CO_2 from a geological storage unit—current status. Int. J. Greenh. Gas Control 22, 272–290.
Matson, J.V., Characklis, W.G., 1976. Diffusion into microbial aggregates. Water Res. 10, 877–885.
McKellar, M., Wardlaw, N.C., 1982. A method of making two-dimensional glass micromodels of pore systems. J. Can. Petrol. 21, 39–41.
Mitchell, A.C., Phillips, A., Hiebert, R., Cunningham, A.B., 2009. Biofilm enhanced subsurface sequestration of supercritical CO_2. Int. J. Greenh. Gas Control 3 (1), 90–99.
Mitchell, A.C., Didderiksen, K., Spangler, L.H., Cunningham, A.B., Gerlach, R., 2010. Microbially enhanced carbon capture and storage by mineral-trapping and solubility-trapping. Environ. Sci. Technol. 44, 5270–5276.
Motegi, C., Tanaka, T., Piontek, J., Brussaard, C.P.D., Gattuso, J.P., Weinbauer, M.G., 2013. Effect of CO_2 enrichment on bacterial metabolism in an Arctic fjord. Biogeosciences 10, 3285–3296.
Nivala, J., Knowles, P., Dotro, G., Garcıa, J., Wallace, S., 2012. Clogging in subsurface-flow treatment wetlands: measurement, modeling and management. Water Res. 46, 1625–1640.
Oule, M.K., Tano, K., Bernier, A.-M., Arul, J., 2006. *Escherichia coli* inactivation mechanism by pressurized CO_2. Can. J. Microbiol. 52, 1208–1217.
Phillips, A.J., Lauchnor, E., Eldring, J., Esposito, R., Mitchell, A.C., Gerlach, R., Cunningham, A.B., Spangler, L.H., 2012. Potential CO_2 leakage reduction through biofilm-induced calcium carbonate precipitation. Environ. Sci. Technol. 47, 142–149.
Robin, M., Behot, J., Sygouni, V., 2012. CO_2 injection in porous media: observations in glass micromodels under reservoir conditions. In: SPE-DOE Improved Oil Recovery Symposium Proceedings, vol. 2, pp. 1025–1039.
Seki, K., Miyazaki, T., Nakano, M., 1998. Effects of microorganisms on hydraulic conductivity decrease in infiltration. Eur. J. Soil Sci. 49 (2), 231–236.
Sen, R., 2008. Biotechnology in petroleum recovery: the microbial EOR. Prog. Energy Combust. Sci. 34 (6), 714–724.
Soudmand-asli, A., Ayatollahi, S.S., Mohabatkar, H., Zareie, M., Shariatpanahi, S.F., 2007. The *in situ* microbial enhanced oil recovery in fractured porous media. J. Petrol. Sci. Eng. 58, 161–172.
Stewart, T., Kim, D.-S., 2004. Modeling of biomass-plug development and propagation in porous media. Biochem. Eng. J. 17, 107–119.
Stumm, W., Morgan, J.J., 1981. Aquatic Chemistry: An Introduction Emphasizing Chemical Equilibria in Natural Waters, 2nd ed. Wiley Interscience, New York.
Sygouni, V., Dimadis, G.C., Chrysikopoulos, C.V., 2015. Assessment of CO_2 injection in fractured calcite rock clogged by *Pseudomonas putida* biofilm. Int. J. Green Technol. 1, 65–72.
Thomas, J.M., Chrysikopoulos, C.V., 2010. A new method for in situ concentration measurements in packed-column transport experiments. Chem. Eng. Sci. 65, 4285–4292.
Tsakiroglou, C.D., Theodoropoulou, M., Karoutsos, V., Papanicolaou, D., Sygouni, V., 2003. Experimental study of the immiscible displacement of shear-thinning fluids in pore networks. J. Colloid Interface Sci. 267, 217–232.
Thullner, M., Zeyer, J., Kinzelbach, W., 2002. Influence of microbial growth on hydraulic properties of pore networks. Transp. Porous Med. 49, 99–122.
Vasiliadou, I.A., Chrysikopoulos, C.V., 2011. Cotransport of *Pseudomonas putida* and kaolinite particles through water-saturated columns packed with glass beads. Water Resour. Res. 47, W02543, http://dx.doi.org/10.1029/2010WR009560.
Vizika, O., Payatakes, A.C., 1989. Parametric experimental study of forced imbibition in porous media. Physicochem. Hydrodyn. 11, 187–204.
Wattle, E., 1942. Culture characteristics of zooglea-forming bacteria isolated from activated sludge and trickling filters. Pub. Health Rep. 57, 1519–1534.
Wang, Z., Shen, Y., Haapasalo, M., 2014. Dental materials with antibiofilm properties. Dent. Mater. 30 (2), e1–e16.
Werth, C.J., Zhang, C., Brusseau, M.L., Oostrom, M., Baumann, T., 2010. A review of non-invasive imaging methods and applications in contaminant hydrogeology research. J. Contam. Hydrol. 113, 1–24.
Wood, E.J.F., 1967. Microbiology of Oceans and Estuaries. Elsevier Oceanography Series, vol. 3. Elsevier Publishing Co., New York, pp. 206–225 (Chapter VIII).
Zhang, J., Davis, T.A., Matthews, M.A., Drews, M.J., LaBerge, M., An, Y.H., 2006. Sterilization using high-pressure carbon dioxide. J. Supercrit. Fluids 38 (3), 354–372.
Zheng, L., Apps, J.A., Zhang, Y., Xu, T., Birkholzer, J.T., 2009. On mobilization of lead and arsenic in groundwater in response to CO_2 leakage from deep geological storage. Chem. Geol. 268, 281–297.
ZoBell, C.E., 1939. Fouling of submerged surfaces and possible preventive procedures. The biological approach to the preparation of antifouling paints. Paint Oil Chem. Rev. 101, 74–77.
ZoBell, C.E., 1943. The effect of solid surfaces upon bacterial activity. J. Bacteriol. 46, 39–56.